Profound change of the near-Earth radiation environment caused by solar superstorms

Yuri Shprits,[1,2] Dmitriy Subbotin,[2] Binbin Ni,[2] Richard Horne,[3] Daniel Baker,[4] and Patrick Cruce[1]

Received 3 February 2011; revised 12 April 2011; accepted 20 April 2011; published 25 August 2011.

[1] The outer radiation belt is often enhanced during storms while the inner belt is usually considered to be unaffected by geomagnetic activity. During the most recent Halloween superstorms, the extreme erosion of the plasmasphere allowed particles to be transported closer to the Earth where they were locally accelerated. Modeling, which now includes transport with resonant acceleration and loss processes and mixed diffusion, shows a rather good correspondence with observations. In this study, we use the same version of the VERB code to model a storm stronger than the Halloween storms, which most likely occurred in the past and may occur in the future. Our simulations indicate that during such a strong event, electrons will be transported into the heart of the inner zone, where they will be accelerated by chorus waves. When the plasmapause extends to larger distances, electrons accelerated by resonant wave-particle interactions in the inner radiation belt will find themselves in a very different plasma environment and strong fluxes may persist for several years after such a storm. Such intensification of the near-Earth plasma environment would substantially decrease satellite lifetimes at LEO. The radiation mitigation strategy for satellites operating in the inner belt should include a consideration of the potential for a dramatic increase in the near-Earth radiation. Such intensification of the near-Earth radiation environment may be truly devastating and would substantially decrease the lifetimes of meteorological, communication, and military satellites.

Citation: Shprits, Y., D. Subbotin, B. Ni, R. Horne, D. Baker, and P. Cruce (2011), Profound change of the near-Earth radiation environment caused by solar superstorms, *Space Weather*, *9*, S08007, doi:10.1029/2011SW000662.

1. Introduction

[2] The electron radiation belts, which are the subject of this study, exhibit a two-zone structure. The inner radiation belt in the equatorial plane is typically located between 1.03 and 2.0 R_E, while the outer belt extends from 4 to 8 R_E. While the outer belt can be episodically enhanced during strong superstorm, the inner belt is usually considered unaffected by geomagnetic storms. The "slot" region (the area between the two belts that is usually devoid of relativistic electrons) is the result of the loss of electrons from the radiation belts to the atmosphere [*Lyons and Thorne*, 1973].

[3] Since high-energy electrons create a hazardous environment for Earth-orbiting satellites and the international space station, understanding the dynamics of the radiation belts and being able to predict the response of the radiation belts to changes in the solar wind is very important [*Baker*, 2002]. In particular, relativistic electrons are responsible for deep dielectric charging in sensitive electronic components and may cause frequent satellite failures and operational problems. The main goal of the current study is to simulate a perfect storm that may occur in the future and estimate the potential effect of such a storm on the near-Earth radiation environment and on the satellites traversing the inner radiation zone.

[4] The outer radiation belt is very dynamic and is influenced by various loss and source processes [*Friedel et al.*, 2002; *Shprits et al.*, 2008a, 2008b]. The loss processes include the scattering of particles by various plasma waves into the atmosphere [*Millan and Thorne*, 2007], the loss of particles through the magnetopause [*Shprits et al.*, 2006a], and the outward radial diffusion of particles under negative radial phase space density gradients [e.g., *Brautigam and Albert*, 2000; *Miyoshi et al.*, 2003; *Shprits et al.*, 2006a]. There are two dominant mechanisms for nonadiabatic electron acceleration to relativistic energies in the heart of the radiation belts: radial diffusion and local acceleration. Radial diffusion involves the net transport of electrons

[1]Institute of Geophysics and Planetary Physics, University of California, Los Angeles, California, USA.
[2]Department of Atmospheric and Oceanic Sciences, University of California, Los Angeles, California, USA.
[3]British Antarctic Survey, Cambridge, UK.
[4]LASP, University of Colorado at Boulder, Boulder, Colorado, USA.

from the highly populated outer magnetosphere toward the inner region where phase space density is depleted by losses. A net diffusive motion inward into the regions of higher magnetic field results in the acceleration of electrons [*Schulz and Lanzerotti*, 1974; *Hudson et al.*, 1999]. Electrons can also be accelerated locally by chorus waves during resonant wave-particle interactions [*Hess et al.*, 1965; *Horne and Thorne*, 1998; *Meredith et al.*, 2002; *Miyoshi et al.*, 2003; *Horne et al.*, 2005a, 2005b; *Summers et al.*, 2007; *Li et al.*, 2007; *Shprits et al.*, 2009a; *Albert et al.*, 2009]. Often storms with a Dst index below 200–300 nT are referred to as superstorms. Such extreme events often provide a very unique opportunity to test the existing models and to understand the physics of radiation belt acceleration and loss [e.g., *Horne et al.*, 2005b; *Shprits et al.*, 2006c; *Loto'aniu et al.*, 2006]. Due to an increase of particle fluxes during superstorms, the probability of satellite failure significantly increases. The relative contribution of each acceleration process during superstorms is still unknown.

[5] In recent years, a number of codes have been developed based on the original formulation of *Lyons et al.* [1972] to evaluate the bounce-averaged quasi-linear scattering rates without making a high-density approximation [e.g., *Glauert and Horne*, 2005; *Albert*, 2003; *Shprits et al.*, 2006d; *Summers et al.*, 2007; *Ni et al.*, 2008; *Shprits and Ni*, 2009]. Since both radial transport [e.g., *Elkington et al.*, 1999; *Hudson et al.*, 1999; *O'Brien et al.*, 2003; *Shprits and Thorne*, 2004] and local diffusion [e.g., *O'Brien et al.*, 2003; *Horne et al.*, 2005b; *Shprits et al.*, 2008b] play important roles, a number of codes capable of combining radial transport and pitch angle and energy diffusion have recently been developed [*Varotsou et al.*, 2005, 2008; *Miyoshi et al.*, 2003; *Jordanova et al.*, 1996, 2003; *Fok et al.*, 2008; *Shprits et al.*, 2008b; *Albert et al.*, 2009].

[6] In the current paper, we start by giving a detailed description of the VERB code [*Shprits et al.*, 2008b, 2009a; *Subbotin and Shprits*, 2009] used in this study. In section 3, we present simulations of radiation belt fluxes at low altitude and a comparison with SAMPEX observations, concentrating on modeling the unusual behavior of radiation belt fluxes in the slot region during the Halloween Superstorms. Section 4 presents simulations of a hypothetical storm, which has likely occurred in the past and may occur in the future, followed by an estimate of what could be the damage to spacecraft from such a storm. Section 5 presents a discussion and conclusions.

2. Code Description

[7] VERB code [*Shprits et al.*, 2006c, 2008b; *Subbotin and Shprits*, 2009; *Shprits et al.*, 2009a] accounts for a number of resonant wave-particle interaction processes that are believed to be dominant in determining the general shape and evolution of the radiation belts. The VERB code models the violation of adiabatic invariants by solving the modified 3-D Fokker-Planck diffusion equation (1) that incorporates energy diffusion, pitch angle scattering, mixed diffusion, and radial diffusion for the drift- and bounce-averaged particle phase space density (PSD) f

$$\frac{\partial f}{\partial t} = L^{*2}\frac{\partial}{\partial L^*}\Big|_{\mu,J}\left(D_{L^*L^*}L^{*-2}\frac{\partial f}{\partial L^*}\Big|_{\mu,J}\right) + \frac{1}{p^2}\frac{\partial}{\partial p}\Big|_{y,L}p^2\left(\langle D_{pp}(y,p)\rangle\frac{\partial f}{\partial p}\Big|_{y,L} + \langle D_{py}(y,p)\rangle\frac{\partial f}{\partial y}\Big|_{p,L}\right) + \frac{1}{T(y)y}\frac{\partial}{\partial y}\Big|_{p,L}T(y)y\left(\langle D_{yy}(y,p)\rangle\frac{\partial f}{\partial y}\Big|_{p,L} + \langle D_{yp}(y,p)\rangle\frac{\partial f}{\partial p}\Big|_{y,L}\right) - \frac{f}{\tau}, \quad (1)$$

where y is the sine of the equatorial pitch angle, p is the particle's momentum, $\langle D_{pp}\rangle$, $\langle D_{py}\rangle$, and $\langle D_{yy}\rangle$ are the bounce- and MLT-averaged components of the diffusion tensor, $T(y) = 1.3802–0.3198\,(y + y^{1/2})$, and τ is the characteristic loss timescale that is assumed to be infinite outside the loss cone and equal to a quarter bounce time inside the loss cone.

[8] In this formulation, momentum diffusion is responsible for the acceleration of electrons, pitch angle scattering produces a loss of electrons to the atmosphere, and radial diffusion redistributes relativistic electron PSD by accelerating electrons during the inward transport and decelerating them during the outward transport. Equation (1) accounts for simultaneous acceleration by both Ultra Low Frequency (ULF) and Very Low Frequency (VLF) waves [*O'Brien et al.*, 2003]. The outer boundary condition is set up at L = 7, while at the inner boundary we assume that there is an absence of electrons at the top of the atmosphere.

[9] There are a number of processes that are not accounted for by this formulation, such as acceleration and loss by nonlinear scattering [e.g., *Inan et al.*, 1978; *Albert*, 1993], loss due to scattering by magnetosonic waves [*Horne et al.*, 2007], electromagnetic ion cyclotron (EMIC) waves [*Albert*, 2003; *Li et al.*, 2007], electrostatic wave scattering [e.g., *Lyons*, 1974], acceleration in the region of the cusp, bounce-resonant acceleration and loss by magnetosonic waves [*Shprits*, 2009], nondiffusive radial transport [e.g., *Ukhorskiy et al.*, 2006], convective transport of the seed population [e.g., *Fok et al.*, 2008], and other processes. While all of these processes may be important and may contribute to the acceleration and loss of electrons and electron transport in the outer regions, in this study we take into account only processes that have been clearly shown to play a dominant role in determining the general morphology of the radiation belts and the global evolution of fluxes.

[10] The 3-D VERB code computes the evolution of fluxes as a function of radial distance, energy, and equatorial pitch angle. The VERB code uses a two-grid formulation, which is described in detail in a recent study [*Subbotin and Shprits*, 2009]. One grid is used for the numerical approximation of the radial diffusion operator

and is constructed so that the first and second adiabatic invariants are conserved along the grid lines. The grid that is used for the computation of acceleration and loss is constructed so that, for a fixed L shell, the momentum and pitch angle plane grid lines are straight and orthogonal to each other. On each time step, we interpolate between the grids using the spline method. The convergence of the numerical method in time and space as well as the accuracy of interpolation has been demonstrated in a recent study [*Subbotin and Shprits*, 2009].

[11] Previous studies that discussed the Halloween solar storms [*Horne et al.*, 2005b, *Shprits et al.*, 2006c] included only 1-D and 2-D modeling, respectively. They presented simulations of the late recovery phase of the storms at a fixed location in the center of the slot region. They did not model radial transport, which provides the seed population. Comparison between observations and model results was very qualitative. Such simplified models can only roughly say if fluxes increase or decrease and also can only roughly show what mechanism is most important. In order to understand the physical processes responsible for the unusual behavior of the radiation belts, we need to quantify the dominant mechanisms in a model. In this study, we account for radial diffusion and pitch angle, energy, and mixed scattering in the 3-D VERB code. We present fluxes integrated over all local pitch angles that can be observed at 850 km in a dipole field inferred from global simulations.

[12] After computing fluxes at all L shells and pitch angles, we select equatorial pitch angles of electrons that can reach SAMPEX altitude and integrate over all local pitch angles at SAMPEX altitude. Such calculation requires a high resolution in pitch angle and energy, and also requires the accurate prediction of the electron pitch angle distributions, especially at low pitch angles. To more accurately resolve small pitch angles, we use a logarithmically spaced high-resolution grid in pitch angle. While the general evolution of fluxes at the equator may be more or less similar to the evolution at SAMPEX altitude, the accurate quantification of fluxes at these small pitch angles also requires the inclusion of mixed diffusion terms [e.g., *Albert and Young*, 2005; *Subbotin et al.*, 2010].

[13] The spectrum of fluxes at the outer boundary of the code is taken from time-averaged observations of fluxes near the geosynchronous orbit from LANL, which cover the energy range from tens of keV to a few MeV and has been described in a recent study [*Shprits et al.*, 2009a]. The lower boundary condition for the momentum diffusion is assumed to be constant as a result of balance between convective sources and losses and is obtained by solving the steady state radial diffusion equation for Kp = 4 for electrons with energies of 10 keV at the outer boundary (L = 7). The outer radial boundary at L = 7 is chosen to be relatively far from the slot region but still mostly in the region where electrons are on closed drift orbits. The lower boundary in energy is also chosen so that the lowest energy level at all L shells is relatively far from the modeled 1.0 MeV electron fluxes. Since convective sources are not explicitly modeled, we cannot choose a boundary at lower energy values since electron transport at these energies is dominated by convection. Ideally, we would like to have the convective source modeled by a kinetic convective code coupled to VERB, which, however, is a very challenging task and will be a subject of future studies.

[14] Since pitch angle scattering is a fast process, we assume that the pitch angle distribution at the lowest energy can be described by a sine function, which cannot significantly affect modeled pitch angle distributions at MeV energies. The upper boundary condition for the momentum diffusion is zero flux at 10 MeV at L = 7. The energy of the upper boundary increases with decreasing L, according to the conservation of the first and second adiabatic invariants. Since fluxes at multi MeV energies are orders of magnitude smaller than at 1 MeV, the neglect of fluxes at energies above 10 MeV cannot affect the diffusive processes that influence 1 MeV electrons. Boundary conditions for the pitch angle diffusion are zero flux at zero pitch angle and zero gradient for the upper boundary near 90°. The initial condition is obtained by solving the steady state radial diffusion equation for Kp = 4. The Fokker-Planck equation (1) is solved for diagonal and mixed terms on the 61 × 101 × 91 grid in radial distance, momentum, and pitch angle, respectively. To account for mixed diffusion terms, we use the bulk implicit method of *Subbotin et al.* [2010]. In the current study, we use a logarithmic grid in momentum, which allows us to accurately resolve energy scales below a few MeV while keeping the grid coarse at ultrarelativistic energies for which phase space density is very small. The pitch angle grid is also taken to be logarithmic to accurately resolve small equatorial pitch angle electrons near the edge of the loss cone that are observed by SAMPEX. The radial grid is chosen to be uniform to account for local acceleration, pitch angle scattering, and radial diffusion that occurs at all L shells.

[15] To minimize the influence of the initial condition on the simulations, the code is first spun up for 7 days to obtain a more realistic state of the radiation belts. During the spin-up time, the outer radiation belt is formed at its typical location. The radial diffusion coefficients are parameterized by the Kp index [*Brautigam and Albert*, 2000]. Pitch angle and energy diffusion coefficients are computed using the UCLA Full Diffusion Code [*Ni et al.*, 2008; *Shprits and Ni*, 2009] for dayside and nightside VLF chorus waves outside the plasmasphere and VLF or Extremely Low Frequency (ELF) plasmaspheric hiss inside the plasmasphere. Since electron loss due to Coulomb scattering is important only in the region below L = 1.3 [*Walt*, 1964; *Abel and Thorne*, 1998] and in this study we concentrate on MeV electron acceleration and loss in the inner zone above L = 1.3, we have neglected the effect of Coulomb scattering in this study.

[16] We assume that the wave power spectral density $B^2(\omega)$ is distributed according to a Gaussian frequency

Table 1. Parameters of Waves Used for Simulations

Type of Wave	B_W (pT)	λ_{max}	Density Model	Percent MLT	Wave Spectral Properties	Distribution in Wave Normal
Dayside chorus	$10^{0.75+0.04\lambda}$. $(2 \cdot 10^{0.73+0.91Kp})^{0.5}/57.6$, for Kp ≤ 2+; $10^{0.75+0.04\lambda}$. $(2 \cdot 10^{2.5+0.18Kp})^{0.5}/57.6$, for 2+ < Kp;	35°	*Sheeley et al.* [2001]	25%	ω_m/Ω_e = 0.2, $\delta\omega/\Omega_e$ = 0.1, ω_{uc}/Ω_e = 0.3, ω_{lc}/Ω_e = 0.1	θ_m = 0°, $\delta\theta$ = 30°, θ_{uc} = 45°, θ_{lc} = 0°.
Nightside chorus	$50 \cdot (2 \cdot 10^{0.73+0.91Kp})^{0.5}/57.6$, for Kp ≤ 2+; $50 \cdot (2 \cdot 10^{2.5+0.18Kp})^{0.5}/57.6$, for 2+ < Kp;	15°	*Sheeley et al.* [2001]	25%	ω_m/Ω_e = 0.35, $\delta\omega/\Omega_e$ = 0.15, ω_{uc}/Ω_e = 0.65, ω_{lc}/Ω_e = 0.05	θ_m = 0°, $\delta\theta$ = 30°, θ_{uc} = 45°, θ_{lc} = 0°.
Plasmaspheric hiss	$40 \cdot Kp/4$	45°	*Carpenter and Anderson* [1992] at L > 2; *Starks et al.* [2008] at L < 2	60%	$\omega_m = 0.55 \cdot 2\pi$ rad kHz, $\delta\omega = 0.3 \cdot 2\pi$ rad kHz, $\omega_{uc} = 2 \cdot 2\pi$ rad kHz, $\omega_{lc} = 0.1 \cdot 2\pi$ rad kHz	θ_m = 45°, $\delta\theta$ = 22.5°, θ_{uc} = 67.5°, θ_{lc} = 22.5°.
Lightning induced whistler waves	1	45°	*Carpenter and Anderson* [1992] at L > 2; *Starks et al.* [2008] at L < 2	100%	$\omega_m = 4.5 \cdot 2\pi$ rad kHz, $\delta\omega = 2 \cdot 2\pi$ rad kHz, $\omega_{uc} = 6.5 \cdot 2\pi$ rad kHz, $\omega_{lc} = 2.5 \cdot 2\pi$ rad kHz	θ_m = 45°, $\delta\theta$ = 22.5°, θ_{uc} = 67.5°, θ_{lc} = 22.5°.
VLF transmitter frequency range 1	0.8	45°	*Carpenter and Anderson* [1992] at L > 2; *Starks et al.* [2008] at L < 2	2.4% × 4	$\omega_m = 17.1 \cdot 2\pi$ rad kHz, $\delta\omega = 0.05 \cdot 2\pi$ rad kHz, $\omega_{uc} = 17.2 \cdot 2\pi$ rad kHz, $\omega_{lc} = 17.0 \cdot 2\pi$ rad kHz	θ_m = 45°, $\delta\theta$ = 22.5°, θ_{uc} = 67.5°, θ_{lc} = 22.5°.
VLF transmitter frequency range 2	0.8	45°	*Carpenter and Anderson* [1992] at L > 2; *Starks et al.* [2008] at L < 2	2.4% × 4	$\omega_m = 22.3 \cdot 2\pi$ rad kHz, $\delta\omega = 0.05 \cdot 2\pi$ rad kHz, $\omega_{uc} = 22.4 \cdot 2\pi$ rad kHz, $\omega_{lc} = 22.2 \cdot 2\pi$ rad kHz	θ_m = 45°, $\delta\theta$ = 22.5°, θ_{uc} = 67.5°, θ_{lc} = 22.5°.

distribution with fixed cutoffs ω_{lc} and ω_{uc}, median value ω_m, and bandwidth $\delta\omega$ [*Lyons et al.*, 1971]:

$$B^2(\omega) = B_w^2 \frac{2}{\sqrt{\pi}\delta\omega}\left(erf\left(\frac{\omega_m - \omega_{lc}}{\delta\omega}\right) + erf\left(\frac{\omega_{uc} - \omega_m}{\delta\omega}\right)\right)^{-1} \cdot \exp\left(-\left(\frac{\omega - \omega_m}{\delta\omega}\right)^2\right), \quad (2)$$

where B_w is the average wave amplitude. We also assume that the wave normal distribution is Gaussian and given by

$$g(X) = \exp\left(-(X - X_m)^2/X_w^2\right), \quad (3)$$

where $X = \tan(\theta)$, $X_m = \tan(\theta_m)$, $X_w = \tan(\delta\theta)$, θ is the wave normal angle, θ_m is the peak wave normal angle, and $\delta\theta$ is a parameter describing the angular width of the distribution.

[17] Diffusion coefficients are computed with the realistic wave parameters shown in Table 1. Wave spectral properties were obtained from a number of statistical studies that were summarized by *Li et al.* [2007]. Distributions in wave normal angle of chorus and hiss waves are taken according to statistical studies from CRRES satellite observations [*Horne et al.*, 2005a; *Meredith et al.*, 2007]. Hiss waves are assumed to be present throughout the inner zone [*Tsurutani et al.*, 1975]. The parameterization of hiss amplitudes is taken empirically from CRRES observations, which were mostly taken in the outer belt and slot region. These estimates are very conservative and may in fact overestimate hiss amplitudes inside the inner belt where a number of cases were observed to be on the scale of 10 pT [*Tsurutani et al.*, 1975]. The scaling of chorus amplitudes with Kp is taken from the analysis of CRRES measurements [*Shprits et al.*, 2007, 2009a, 2009b]. Information about lightning-generated whistlers and VLF transmitters are modeled following a theoretical study [*Abel and Thorne*, 1998] and are scaled following a recent observational study [*Starks et al.*, 2008].

[18] In this study, we do not account for scattering by EMIC waves. These waves may clearly contribute to the loss of electrons at lower L shells and their inclusion may improve the results of simulations. Typical storm time EMIC wave amplitudes of 1–10 nT cause strong diffusion scattering, which leads to significant losses of relativistic electrons [*Meredith et al.*, 2003; *Ukhorskiy et al.*, 2010].

[19] We assume that the plasmapause is axisymmetric. Inclusion of the MLT-dependent plasmapause as well as the modeling of the plasmapause location based on the solar wind conditions will be subjects of future research. The location of the plasmapause L_{pp} is given by [*Carpenter and Anderson*, 1992]

$$L_{pp} = 5.6 - 0.46\,Kp_{max}, \quad (4)$$

where Kp_{max} is the maximum value of Kp over the preceding 24 h. A visual comparison of the plasmapause value with the plasmapause obtained from IMAGE data [*Baker et al.*, 2004] shows that a simple Kp-based parameterization can in general reproduce the dynamics of the plasmapause quite well.

[20] When the Kp index exceeds 6, the fluxes at the outer radial boundary (L = 7) are scaled by

$$B_f = 10^{((-1)\cdot Kpmax/5)}, \quad (5)$$

where B_f is the scaling coefficient, which is used in a manner similar to the method of *Brautigam and Albert* [2000]. This scaling is used to simulate the loss of electrons to the magnetopause. This time-dependent boundary condition is scaled so that the time average of the log of fluxes over the simulation time is the same as the constant boundary condition used in previous studies [*Subbotin and Shprits*, 2009; *Shprits et al.*, 2009a]. This variation of fluxes models the nonadiabatic dropouts often observed during a typical storm.

3. Simulations of the Halloween Storms

[21] The Halloween storms of 2003 [*Baker et al.*, 2004; *Horne et al.*, 2005b; *Shprits et al.*, 2006c] presented one of the most interesting episodes of solar activity ever observed during the space age. Figure 1a shows SAMPEX observations of 2–6 MeV electron fluxes during 25 October to 21 November 2003 and compares them to modeled electron fluxes at an altitude of 850 km simulated by the VERB diffusion code (Figure 1b).

[22] Comparison of SAMPEX observations with VERB code simulations shows that the model driven by only the Kp index can predict the general dynamics of the radiation belts. The code accurately predicts the dynamics of the belt and the locations of the peak of radiation belt fluxes between 27 October and 11 November (Figure 1b). When Kp dramatically increased between 29 October and 30 October, a decrease in flux at the outer boundary produced losses at high L shells, while increases in radial diffusion rates allowed electrons from the outer belt to penetrate deep inside the slot region, down to $L = 2$. The electrons that diffuse radially into the slot region [*Loto'aniu et al.*, 2006] during these superstorms find themselves outside the plasmasphere [*Baker et al.*, 2004], and are locally accelerated by the VLF chorus waves to reach peak values inside the slot region on 1–2 November in both observations and simulations. Note that VLF waves are excited by energetic electrons that are sporadically injected for days or even weeks. Such injections should lead to chorus generation for extended periods of time [*Tsurutani et al.*, 2006]. In this study, Kp-dependent VLF chorus parameterizations are chosen according to parameterizations given in Table 1. Parameterized chorus wave amplitudes on the day side reach 141 pT.

[23] After 2 November, when the plasmapause extended to higher L shells, electrons in the slot region were scattered by plasmaspheric hiss waves, lightning-generated whistler mode waves, and anthropogenic whistler mode waves, all of which can induce decay in electron fluxes on the time scale of 5–10 days. After 11 November, the outer radiation belt was reformed at its usual location outside the slot region. When the Kp index increased again on 20 November to a value of 9, which is its maximum value, the radial diffusion increased accordingly and high-energy electrons again penetrated into the inner belt.

[24] A careful comparison of observations (Figure 1a) and simulations (Figure 1b) shows that the VERB code cannot exactly reproduce the location of the reformed outer radiation belt and that there are differences in the amplitudes of flux enhancements. The exact location of the outer belt depends on the balance between radial diffusion and losses and may also depend on the spatial extent of various magnetospheric waves and the location of the plasmapause. Since most of these parameters are taken from statistical studies and the simulation results may significantly depend on the assumed wave models [*Shprits et al.*, 2006d] and assumed outer boundary conditions [*Shprits et al.*, 2009a], we can only expect the code to approximately reproduce the magnitudes of fluxes and locations of the peaks of fluxes.

[25] However, the code accurately reproduces the refilling of the slot region, which is the main focus of the current study. During the main phase of the storms modeled in this study, the VERB code overestimates fluxes at low L shells close to the plasmapause where EMIC waves may provide additional losses. Currently the statistical properties of EMIC waves during storms are not known nor is it known how often these waves can reach frequencies close to the local ion gyro frequency, which is necessary to scatter relativistic electrons.

4. Simulations of an Extremely Strong Superstorm

[26] Our observations of the radiation belts in space are limited to only 3 to 4 solar cycles. Coronal mass ejections (CME) on the Sun may produce storms even stronger than those observed in space over the last 3 to 4 decades. In situ observational data are very limited, however, indirect measurements of the intensity of a storm, taken from ground measurements or visual measurements, date back to the 17th century. While during a moderate storm the ground disturbance of the magnetic field is on the scale of −50 to −100 nT, during the Halloween superstorms of October–November 2003, when the slot region between the two belts was populated, the disturbances on the ground were on the scale of −400 nT. The geomagnetic storm in September 1859 was the strongest ever observed as well as the first to be observed visually. This "perfect storm" is usually called the 'Carrington' storm after one of the first witnesses to observe and document this storm [*Carrington*, 1859]. Using measurements of the magnetic field component from the Colaba Observatory in Bombay/Mumbai taken during 1846–1867, *Tsurutani et al.* [2003] inferred that disturbances on the ground produced by such a storm may have exceeded 1600 nT, which is approximately four times as large as was observed during the Halloween storms in 2003. Other superstorms, which were likely weaker than the 'Carrington' storm, occurred

in 1890, 1909, 1946, 1956 and 1960, all before extensive in situ observations were available [*Shea*, 2006].

[27] Since our simulations are driven solely by the evolution of the geomagnetic index Kp, we can use the code to predict the outcome of a very strong superstorm, similar to the Carrington storm, which may hypothetically occur in the future. Figure 2b shows the results of the simulations of a Carrington-type superstorm and compares them to the original simulation of the Halloween storms (Figure 2a) described in detail above. To simulate realistic prestorm

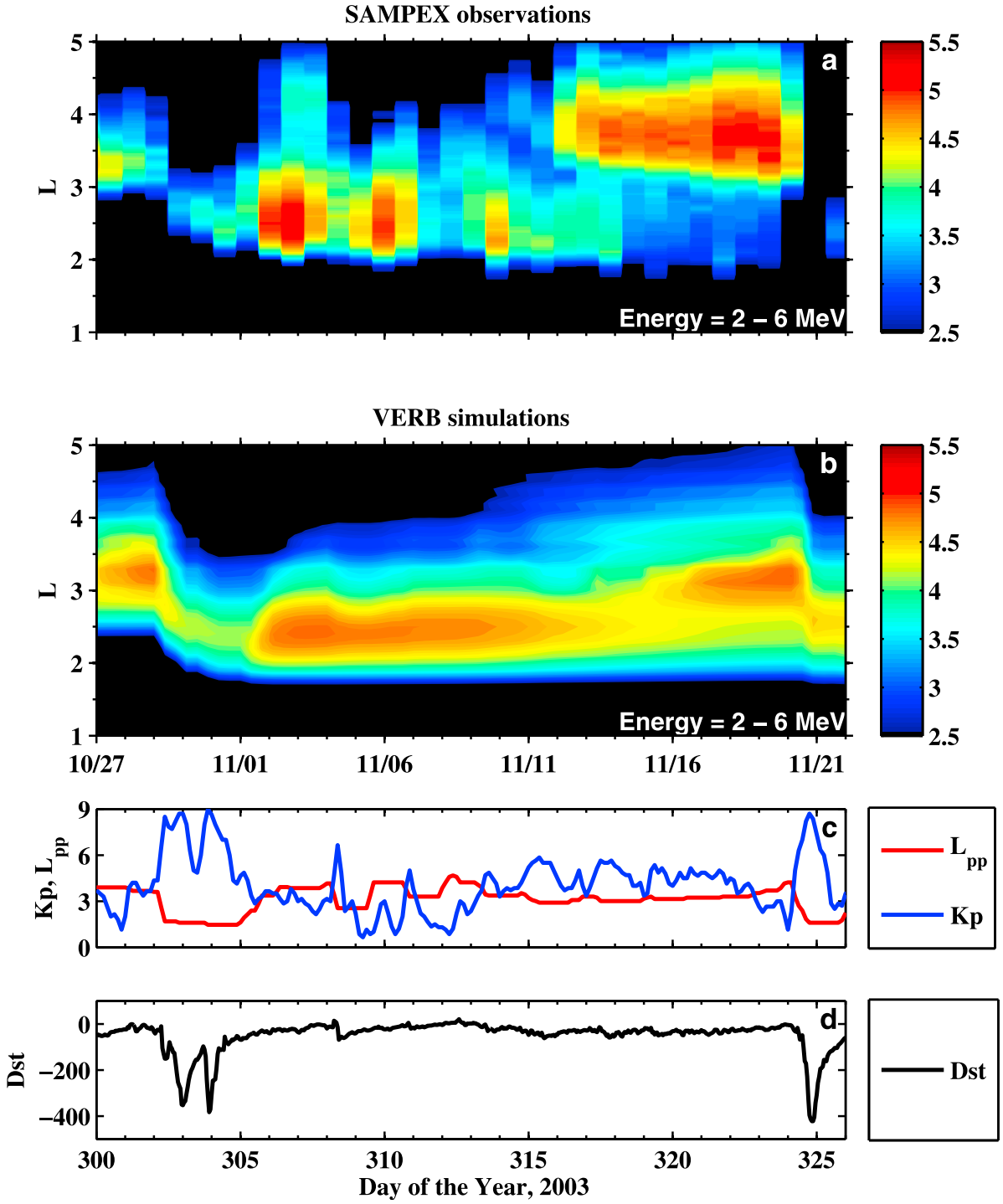

Figure 1

and poststorm conditions, we take the original time series of the Kp index used for the simulations described in section 2 and increase the driver of parameterizations (Kp index) by two when the Kp index exceeds 7.

[28] The plasmapause location plays a critical role in determining the dynamical evolution of fluxes during superstorms. Local acceleration of electrons in the heart of the inner belt is only possible if plasmapause is eroded to L = 1.5 and the plasma density is relatively low outside of the plasmapause. Radial diffusion will also be required to produce inner zone acceleration since it supplies the seed population for the local acceleration into the heart of the inner zone. For radial diffusion to be efficient, ULF waves should extend to lower L shells, a phenomenon that has been observed during very strong superstorms [*Loto'aniu et al.*, 2006]. In this study, we only accounted for radial scattering produced by magnetic fluctuations of the ULF waves, which is not very efficient at low L shells. Our scattering rates most likely underestimate realistic radial diffusion rates in the inner zone. To provide a seed population of electrons for local acceleration in the inner belt we increased the driver of assumed parameterizations of waves, Kp, by 2. Clearly all of the parameterizations we used, including the parameterization of the plasmapause position, parameterizations of VLF wave activity, and the parameterization of radial diffusion rates were not derived for such strong storms. Future research should concentrate on providing better physics-based parameterizations of the diffusion coefficients and plasmapause location during such strong events.

[29] The extrapolated parameterizations to higher Kp may not be completely realistic. However, the inner belt fluxes will be increased for several years, independent of the assumed parameterizations, as long as the plasmasphere is depleted to reach very low L values below 1.5 at least at some MLT sector and ULF waves are present down to low L values. Lifetimes are very long at L = 1.5 and fluxes can persist for a long time. During the Halloween storms the plasmapause was moved below L = 2. During the Carrington storm, the plasmasphere was eroded and compressed down to the unprecedentedly low L value of 1.3 [*Tsurutani et al.*, 2003]. For our simulations of a superstorm, we use parameterization (4) but do not allow the plasmapause to be below L = 1.3. Determining the solar wind conditions that produce such an extreme erosion of the plasmasphere is a challenging task and should be a subject of future research.

[30] While the main phase dropout of fluxes in the simulated 'perfect storm' is stronger than it is for the simulated Halloween storm, electrons can still penetrate to lower L shells, deep into the inner radiation zone. Severe erosion of the plasmasphere would allow ULF waves, which may be otherwise reflected at the plasmapause, to penetrate to such low L shells [*Hartinger et al.*, 2010]. These electrons are locally accelerated further, which results in stronger fluxes of 2–6 MeV electrons and a broader spatial extent of fluxes. The modeled storm on day 324 can also diffuse electrons to such low L values and can further increase fluxes at radial distances of less than 1.5 Earth radii.

[31] The superstorm simulations shown in Figure 2b predict a sudden increase in fluxes at the inner edge of the slot region (L = 2) and deep in the heart of the inner zone (L = 1.5). The main difference between the evolutions of fluxes is that at the outer edge of the inner zone fluxes decay on the timescale of 5–10 days, while fluxes in the heart of the inner zone remain practically unchanged during the simulation of the storm. A modeled consequence of a new flare on day 324 further increases fluxes at L = 1.5.

[32] During a perfect storm, when the plasmapause moves below L = 1.5, in the region of the inner belt the plasma density is relatively low and the magnetic field is very strong. In this plasma environment electrons can be efficiently accelerated by ULF and VLF waves in a manner similar to their acceleration during the Halloween storms but at lower L shells. Note that the diffusion coefficients exhibit a complicated nonlinear dependence on L shell, density, and magnetic field. Diffusion is time–dependent and depends on gradients in energy, pitch angle, and radial distance. Only detailed modeling can predict the evolution of fluxes during such an unusual event.

[33] After the plasmapause retreats to higher radial distances, plasma density above 1.3 Earth radii significantly increases. In the heart of the inner zone, resonant scattering by hiss waves inside the plasmasphere becomes much less efficient after the refilling of the plasmasphere. The gyrofrequency at L = 1.5 is four times higher than at L = 2 and 1 MeV particles are not in first order resonance with hiss waves. Note that the first order resonance produces dominant scattering [e.g., *Shprits and Ni*, 2009]. In the heart of the inner zone, only multi MeV electrons can sufficiently Doppler shift the wave frequency to be in first order resonance with hiss waves. At L = 1.5, electrons can

Figure 1. (a) SAMPEX observations of 2–6 MeV electron fluxes in ($\log_{10}(\mathrm{cm}^{-2}\ \mathrm{sr}^{-1}\ \mathrm{sec}^{-1})$) during the 2003 Halloween storms, DOY 300–326 (27 October to 22 November) 1/2 day averaged. Fluxes are presented as a function of time and L shell. Averaging is applied to eliminate periodic variations associated with the spacecraft passing over the regions with weak magnetic fields usually referred to as the South Atlantic Anomaly. (b) VERB code simulations of the dynamics of the radiation belts 2–6 MeV electron omnidirectional fluxes modeled at the altitude of 850 km in a dipole field in ($\log_{10}(\mathrm{cm}^{-2}\ \mathrm{sr}^{-1}\ \mathrm{sec}^{-1})$). A one day moving average is applied. Unlike in the radial diffusion studies [*Miyoshi et al.*, 2003; *Shprits et al.*, 2006a] in which data was used at the outer radial boundary, the VERB code used for this study does not utilize observations and is driven by Kp index only. The outer boundary condition is set up at L = 7 and its variation is parameterized by Kp index. (c) Evolution of the Kp index used for parameterizations of waves and modeled plasmapause location Lpp [*Carpenter and Anderson*, 1992]. (d) Evolution of Dst index.

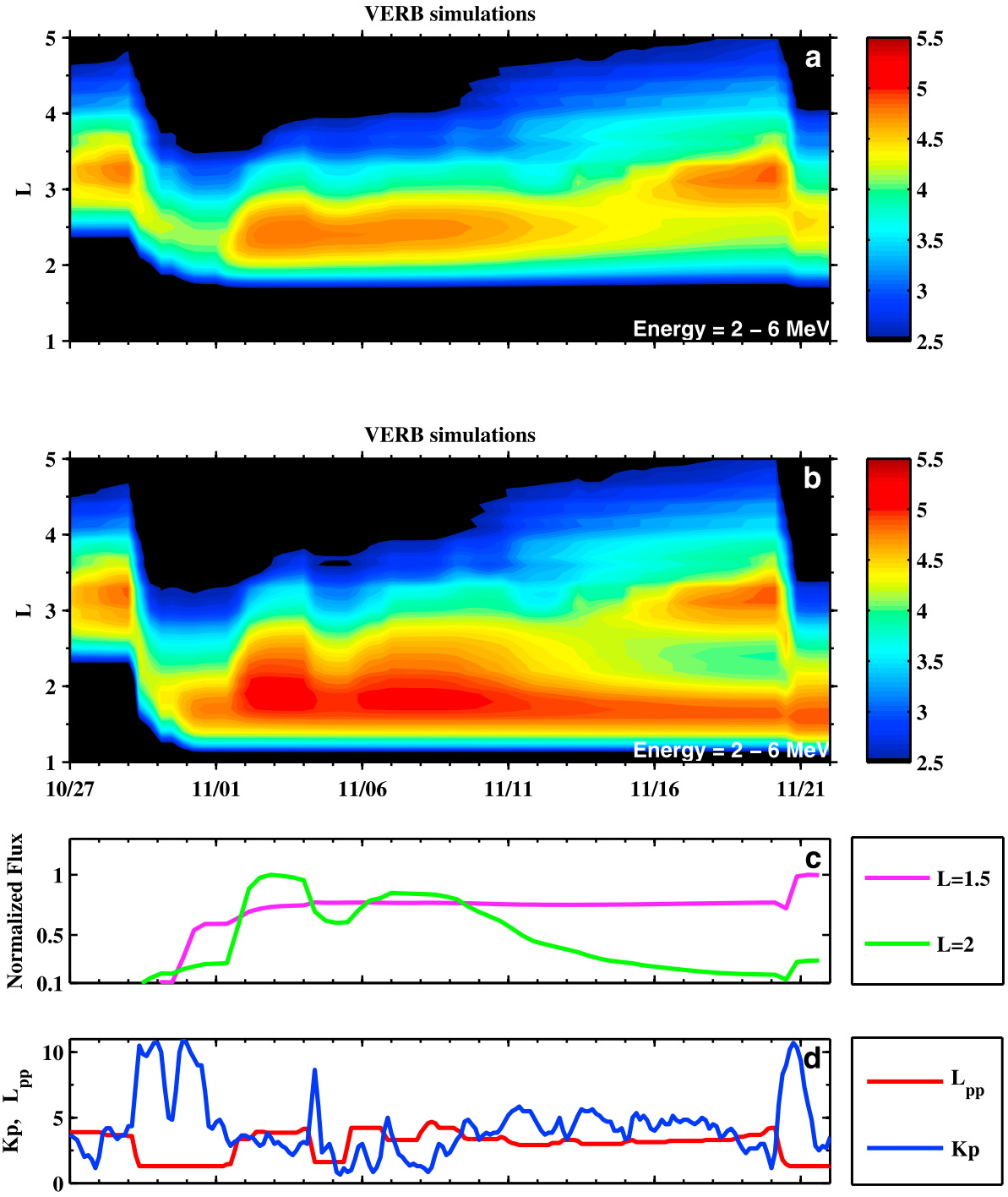

Figure 2. (a) VERB code simulations of the dynamics of the radiation belts 2–6 MeV electron omnidirectional fluxes at the altitude of 850 km in ($\log_{10}$(cm^{-2} sr^{-1} sec^{-1})) for the 2003 Halloween storm. (b) Same as Figure 2a but during a superstorm with Kp used for parameterizations increased by 2 at all times when the Kp index is greater than 7. (c) Evolution of 2–6 MeV radiation belt electron fluxes at the altitude of 850 km for L = 1.5 and L = 2 normalized to the maximum value of the fluxes for the modeled perfect storm. (d) Evolution of the driver of the simulations derived from Kp index and modeled plasmapause location Lpp. The original time series of Kp index used for the simulations described in section 2 was increased by two when Kp index exceeded 7.

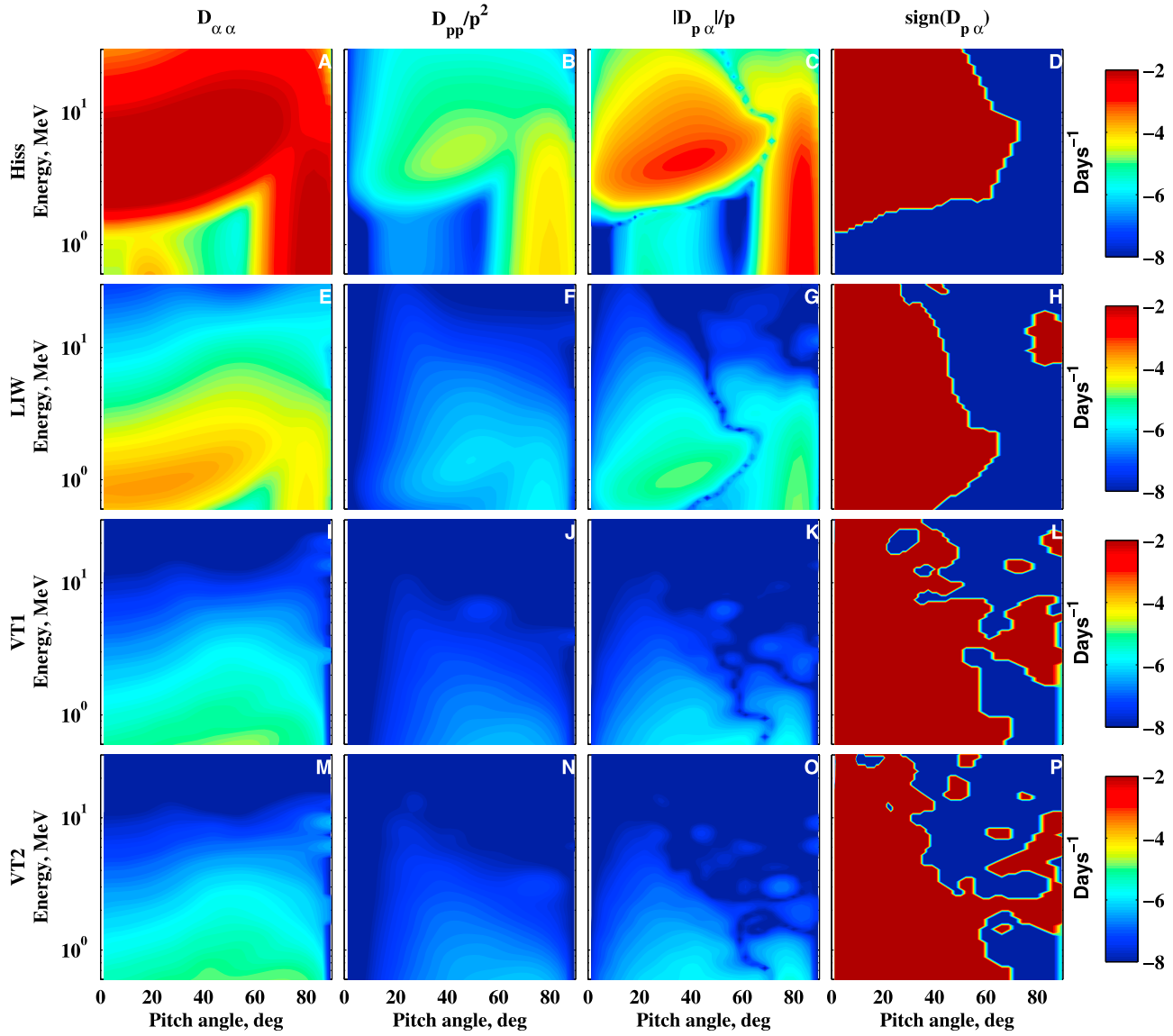

Figure 3. (a, e, i, m) Pitch angle, (b, f, j, n) energy, and (c, g, k, o) mixed bounce averaged diffusion coefficients and (d, h, l, p) the sign of the mixed diffusion coefficients, for hiss (Figures 3a–3d), lightning generated whistlers (Figures 3e–3h), and two models of VLF transmitters (Figures 3i–3l and Figures 3m–3p). Diffusion coefficients are computed using wave spectral properties specified in Table 1 for L = 1.5.

be only scattered by the high-order resonances which results in extremely long lifetimes.

[34] Assuming an exponential decay, the electron lifetime can be calculated from diffusion coefficients [*Shprits et al.*, 2006b]. Diffusion coefficients are computed for the whistlers produced by VLF transmitters, lightning-generated whistlers, and plasmaspheric hiss waves with the parameters taken from Table 1, and the results are shown in Figure 3 for L = 1.5.

[35] Since radial diffusion rates at these L shells are very weak, on the scale of 10^{-7} (R_E^2/day) [*Walt and Newkirk*, 1968], the equilibrium decay rates can be estimated using the value of the inverse pitch angle diffusion coefficient near the edge of the loss cone [*Shprits et al.*, 2006b; *Albert and Shprits*, 2009]. The inverse value of the diffusion coefficient near the edge of the loss cone gives a decay rate of approximately 5 years.

5. Estimation of the Radiation Dose

[36] High-energy electrons create a hazardous environment for Earth-orbiting satellites and the international

space station; understanding the dynamics of the radiation belts and being able to predict the response of the radiation belts to changes in the solar wind is very important [*Baker*, 2002; *Tsurutani et al.*, 2006]. In particular, relativistic electrons are responsible for deep dielectric charging in sensitive electronic components and cause frequent satellite failures and operational problems [*Lanzerotti*, 2001].

[37] To estimate the damage of a potential intensification of particle interactions with an idealized spacecraft, we used Open Source Monte Carlo particle simulation software from the CERN project called "GEANT4" [*Agostinelli et al.*, 2003]. We approximated the shielded electronics of a spacecraft as a silicon sphere with a diameter of 10 cm, shielded by a 2 mm aluminum shell. Simulated electrons with 1000 different initial energy values between 1 MeV and 10 MeV were fired at the center of the sphere from an initial position just on the outer surface of the aluminum shielding. For each of the initial energy values, 1000 electrons were fired and their average energy deposition in the silicon at each energy value was recorded. Our GEANT4 simulation models a number of standard and electromagnetic processes including transportation, multiple scattering, the photoelectric effect, and bremsstrahlung.

[38] The L shells, the ratio of the magnetic field at the satellite orbit to the equatorial magnetic field (B/B_0), and the time spent in each L shell were calculated for a SAMPEX-like orbit (high inclination, low eccentricity, less than 1000 km altitude). Omnidirectional differential electron fluxes (#/cm^2/sec/MeV) over the model orbit for normal conditions at solar maximum were found using NASA's statistical AE8Max model [*Vette*, 1991]. A typical ionizing dose per second (MeV/kg/sec) was determined for AE8Max fluxes at each L shell and for each value of the ratio of the magnetic field B to the equatorial value of the magnetic field B_0 by integrating the energy deposited multiplied by AE8Max fluxes and scaled by the surface area to volume ratio of the sphere and the density of silicon in kg/cm^3.

$$Dose(L(t), B/B_0(t)) = \frac{1}{0.00233}\frac{1}{r}\int_{E=1}^{10} AE8\mathrm{Max} \cdot (E, L(t), B/B_0(t))Edep(E)dE, \quad (6)$$

where t is the time along the orbit and Edep(E) is the energy deposited per electron with initial energy E. The function Edep(E) was determined using GEANT4 modeling. The average dose per orbit was determined by averaging the dose over the total orbit time and converting from MeV/kg/sec to kilorads/sec

$$AverageDose = t_{end}^{-1}\int_{t=0}^{t_{end}} DOSE(L(t), B/B_0(t))dt. \quad (7)$$

Model dose per second was determined using the same method, except that the increased fluxes due to superstorm conditions were combined with AE8Max fluxes.

$$DOSE(L(t), B/B_0(t)) = \frac{1}{0.00233}\frac{1}{r}\int_{E=1}^{10} TotalFlux(E, L(t), B/B_0(t)) \cdot EDEP(E)dE \quad (8)$$

with

$$TotalFlux(E, L(t), B/B_0(t)) = SuperStorm(E, L(t), B/B_0(t)) \quad if 1.3 \le L(t) \le 1.5 \quad (9)$$

$$TotalFlux(E, L(t), B/B_0(t)) = AE8\mathrm{Max}(E, L(t), B/B_0(t)) \quad if\ L(t) < 1.3\ or\ L(t) > 1.5 \quad (10)$$

where TotalFlux(E, L(t), B/B_0(t)) is a piecewise function used to describe the omnidirectional, energy differential flux during a superstorm so that it can be compared to the background flux.

[39] Our modeling shows that a superstorm could increase the dose from electrons to more than 17.1 kilorads/yr for a spacecraft with 2 mm aluminum shielding in a SAMPEX-like orbit (550 × 675 km, 82 deg inclination). To estimate average fluxes in a SAMPEX-like orbit we used a Space Environment Information System (SPENVIS) code, provided by the European Space Administration for a spacecraft with 2 mm aluminum shielding. The estimated total ionizing dosing by SPENVIS is 2.67 kilorad/yr (2.48 from electrons and bremsstrahlung, and 0.19 from protons) during the solar maximum.

[40] Our dose estimates clearly show that, under rather conservative assumptions, a spacecraft in a low Earth orbit could see a decrease in lifetime by a factor greater than 6.4 due to radiation dosage. Spacecraft with less than a 2 mm aluminum shielding equivalent or in higher risk orbits (larger eccentricities or higher mean altitudes) could see increases in radiation dosage that are significantly greater than our modeled results.

[41] As part of a radiation mitigation strategy, a radiation tolerant spacecraft with a design margin for our relatively benign model orbit might include 2 mm aluminum shielding and radiation tolerant components with a 15 kilorad lifetime. Such a satellite would see the reduction of its average lifetime from 5.6 years to 0.85 years after a superstorm discussed in this study.

6. Conclusions

[42] Three-dimensional simulations with the VERB code of the Halloween storms confirm results obtained previously using simpler models and quantitatively reproduce the unusual dynamics of the radiation belts in the slot region. The initial injection of the electrons, which are brought by radial diffusion, is followed by local accelera-

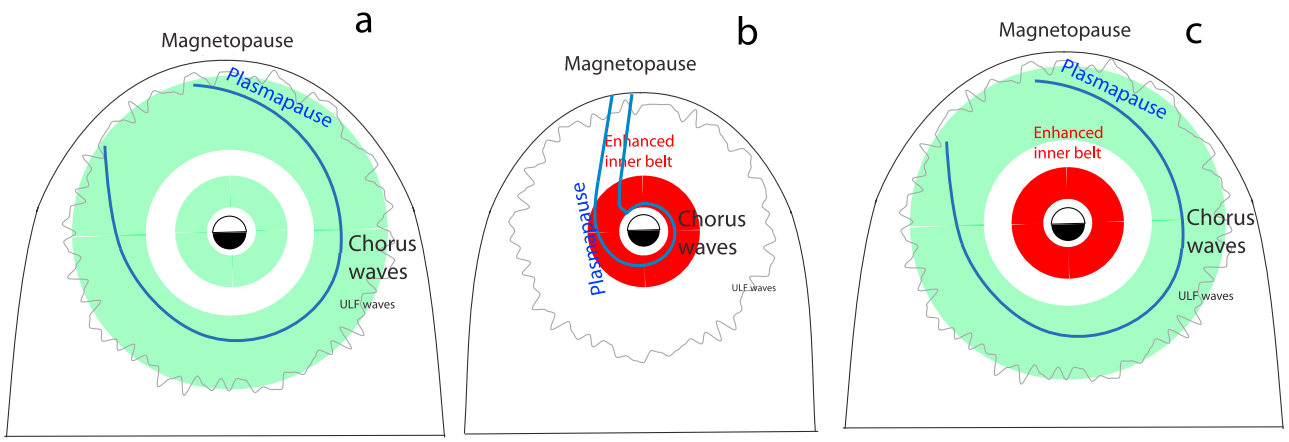

Figure 4. Illustration of the evolution in the Earth's radiation belt fluxes due to a superstorm that compresses the plasmapause below 1.5 Earth radii. Color indicates the intensity of the radiation belt fluxes. (a) Typical two zone structure of the Earth's radiation belts; (b) acceleration of particles during the superstorm, intensification of the inner belt, and depletion of the outer belt; and (c) increased inner belt fluxes after the superstorm which may persist for several years. The green color indicates the average amplitude of the radiation belt fluxes. The blue line shows the plasmapause, which is usually outside the slot region and assures that local acceleration may only increase fluxes in the outer radiation belt. During the Halloween storms the plasmapause was eroded and compressed to only 2 R_E, which did not allow electrons to penetrate into the safe zone below 1.5 R_E.

tion, which produces an unusual radiation belt in the slot region. Simulations of the VERB code including mixed diffusion with Kp-driven parameterizations for the radial diffusion rates, VLF/ELF scattering rates, the plasmapause location, and the outer boundary condition near geosynchronous orbit favorably compare to the observations on SAMPEX, allowing for the simulation of even stronger storms. Our simulations of even stronger storms, which may occur in the future and most likely occurred in the past, show that if the plasmasphere is compressed to 1.3 R_E, as it was during the Carrington storm, relativistic electrons will be injected by the radial diffusion into the heart of the inner belt, where they can be efficiently accelerated by chorus waves. Enhanced radiation belt fluxes at such low L shells are likely to persist for up to a decade due to the slow scattering by waves inside the plasmasphere.

[43] These results are consistent with the early observations of the electron fluxes after the Starfish nuclear detonation, which populated an artificial radiation belt at L ~ 1.3 as observed by Injun 1. Observations of the artificial radiation belt [*Paulikas et al.*, 1967] yield a lifetime of ~265 days at L = 1.3 for electrons above 4.5 MeV.

[44] One reason that these lifetimes are shorter than the ones estimated in our study may be that, at L = 1.3, Coulomb collisions may start to become important and may decrease the electron lifetimes. The second reason may be uncertainty in the amplitudes and spectral characteristics of plasma waves. Also, right after injection, electrons may decay at a slightly faster rate until they reach the equilibrium exponential decay rates that correspond to the longest lived eigenmode.

[45] Figure 4 illustrates the general structure of the radiation belts before (Figure 4a), during (Figure 4b), and after (Figure 4c) such storms. During a superstorm, as described above, the plasmapause is eroded and compressed down to 1.3 R_E, which allows ULF waves to penetrate into the inner belt and diffuse electrons radially much closer to Earth. Local acceleration in the inner belt, where the magnetic field is strong and the plasma density is low, enhances inner radiation belt fluxes and will make them several orders of magnitude higher than the outer radiation belt fluxes, depicted as a red belt in Figures 4b and 4c.

[46] The estimated radiation dose on a typical spacecraft will significantly increase after the types of superstorms described in this study. The lifetime of a typical satellite may decrease to less than one year. Spacecraft engineers should include the scenario of a profound intensification of the inner zone radiation environment into their radiation mitigation strategy. The potential economic loss from such a storm may be devastating. Enhancements of the inner belt will mostly affect satellites in polar and low Earth orbit, which include but are not limited to weather, military, and telecommunication satellites. Measurements made by the upcoming NASA Radiation Belt Storm Probe (RBSP) will allow us to better quantify the acceleration processes, improve our current understanding of the dynamics of the radiation belts, and help us find ways to predict the radiation environment and find methods to mitigate the impact of such superstorms.

[47] **Acknowledgments.** This work was supported by the USAF Young Investigator Research grant FA9550-08-1-0140, NSF GEM grant ATM-0603191, and NASA grant NNX09AF51G. The authors would like to thank Jerry Goldstein, Martin Walt, Ryan Caron, and Viacheslav Merkin for useful discussions.

References

Abel, B., and R. M. Thorne (1998), Electron scattering loss in Earth's inner magnetosphere. 1: Dominant physical processes, *J. Geophys. Res.*, *103*(A2), 2385–2396, doi:10.1029/97JA02919.

Agostinelli, S., et al. (2003), GEANT 4—A simulation toolkit, *Nucl. Instrum. Methods, Sect. A*, *506*, 250–303.

Albert, J. M. (1993), Cyclotron resonance in an inhomogeneous magnetic field, *Phys. Fluids B*, *5*(8), 2744–2750, doi:10.1063/1.860715.

Albert, J. M. (2003), Evaluation of quasi-linear diffusion coefficients for EMIC waves in a multispecies plasma, *J. Geophys. Res.*, *108*(A6), 1249, doi:10.1029/2002JA009792.

Albert, J. M., and Y. Y. Shprits (2009), Estimates of lifetimes against pitch angle diffusion, *J. Atmos. Sol. Terr. Phys.*, *71*, 1647–1652, doi:10.1016/j.jastp.2008.07.004.

Albert, J. M., and S. L. Young (2005), Multidimensional quasi-linear diffusion of radiation belt electrons, *Geophys. Res. Lett.*, *32*, L14110, doi:10.1029/2005GL023191.

Albert, J. M., N. P. Meredith, and R. B. Horne (2009), Three-dimensional diffusion simulation of outer radiation belt electrons during the 9 October 1990 magnetic storm, *J. Geophys. Res.*, *114*, A09214, doi:10.1029/2009JA014336.

Baker, D. N. (2002), How to cope with space weather, *Science*, *297*(5586), 1486–1487, doi:10.1126/science.1074956.

Baker, D. N., S. G. Kanekal, X. Li, S. P. Monk, J. Goldstein, and J. L. Burch (2004), An extreme distortion of the Van Allen belt arising from the "Hallowe'en" solar storm in 2003, *Nature*, *432*(7019), 878–881, doi:10.1038/nature03116.

Brautigam, D. H., and J. M. Albert (2000), Radial diffusion analysis of outer radiation belt electrons during the October 9, 1990, magnetic storm, *J. Geophys. Res.*, *105*(A1), 291–309, doi:10.1029/1999JA900344.

Carpenter, D. L., and R. R. Anderson (1992), An ISEE/whistler model of equatorial electron density in the magnetosphere, *J. Geophys. Res.*, *97*(A2), 1097–1108, doi:10.1029/91JA01548.

Carrington, R. C. (1859), Description of a singular appearance seen in the Sun on September 1, 1859, *Mon. Not. R. Astron. Soc.*, *20*, 13–15.

Elkington, S. R., M. K. Hudson, and A. A. Chan (1999), Acceleration of relativistic electrons via drift-resonant interaction with toroidal-mode Pc-5 ULF oscillations, *Geophys. Res. Lett.*, *26*(21), 3273–3276.

Fok, M.-C., R. B. Horne, N. P. Meredith, and S. A. Glauert (2008), Radiation Belt Environment model: Application to space weather nowcasting, *J. Geophys. Res.*, *113*, A03S08, doi:10.1029/2007JA012558.

Friedel, R. H. W., G. D. Reeves, and T. Obara (2002), Relativistic electron dynamics in the inner magnetosphere—A review, *J. Atmos. Sol. Terr. Phys.*, *64*, 265–282, doi:10.1016/S1364-6826(01)00088-8.

Glauert, S. A., and R. B. Horne (2005), Calculation of pitch angle and energy diffusion coefficients with the PADIE code, *J. Geophys. Res.*, *110*, A04206, doi:10.1029/2004JA010851.

Hartinger, M., M. B. Moldwin, V. Angelopoulos, K. Takahashi, H. J. Singer, R. R. Anderson, Y. Nishimura, and J. R. Wygant (2010), Pc5 wave power in the quiet-time plasmasphere and trough: CRRES observations, *Geophys. Res. Lett.*, *37*, L07107, doi:10.1029/2010GL042475.

Hess, W. N., G. D. Mead, and M. P. Nakada (1965), Advances in particles and field research in the satellite era, *Rev. Geophys.*, *3*(4), 521–570, doi:10.1029/RG003i004p00521.

Horne, R. B., and R. M. Thorne (1998), Potential waves for relativistic electron scattering and stochastic acceleration during magnetic storms, *Geophys. Res. Lett.*, *25*(15), 3011–3014, doi:10.1029/98GL01002.

Horne, R. B., R. M. Thorne, S. A. Glauert, J. M. Albert, N. P. Meredith, and R. R. Anderson (2005a), Timescale for radiation belt electron acceleration by whistler mode chorus waves, *J. Geophys. Res.*, *110*, A03225, doi:10.1029/2004JA010811.

Horne, R. B., et al. (2005b), Wave acceleration of electrons in the Van Allen radiation belts, *Nature*, *437*(7056), 227–230, doi:10.1038/nature03939.

Horne, R. B., R. M. Thorne, S. A. Glauert, N. P. Meredith, D. Pokhotelov, and O. Santolík (2007), Electron acceleration in the Van Allen radiation belts by fast magnetosonic waves, *Geophys. Res. Lett.*, *34*, L17107, doi:10.1029/2007GL030267.

Hudson, M. K., S. R. Elkington, J. G. Lyon, C. C. Goodrich, and T. J. Rosenberg (1999), Simulation of radiation belt dynamics driven by solar wind variation, in *Sun-Earth Plasma Connections*, *Geophys. Monogr. Ser.*, vol. 109, edited by J. L. Burch, R. L. Carovillano, and S. K. Antiochos, pp. 171–182, AGU, Washington, D. C.

Inan, U. S., T. F. Bell, and R. A. Helliwell (1978), Nonlinear pitch angle scattering of energetic electrons by coherent VLF waves in the magnetosphere, *J. Geophys. Res.*, *83*(A7), 3235–3253.

Jordanova, V. K., L. M. Kistler, J. U. Kozyra, G. V. Khazanov, and A. F. Nagy (1996), Collisional losses of ring current ions, *J. Geophys. Res.*, *101*(A1), 111–126, doi:10.1029/95JA02000.

Jordanova, V. K., A. Boonsiriseth, R. M. Thorne, and Y. Dotan (2003), Ring current asymmetry from global simulations using a high-resolution electric field model, *J. Geophys. Res.*, *108*(A12), 1443, doi:10.1029/2003JA009993.

Lanzerotti, L. J. (2001), Space weather effect on technologies, in *Space Weather*, *Geophys. Monogr. Ser.*, vol. 125, edited by P. Song, H. J. Singer, and G. L. Siscoe, pp. 11–22, AGU, Washington, D. C.

Li, W., Y. Y. Shprits, and R. M. Thorne (2007), Dynamic evolution of energetic outer zone electrons due to wave-particle interactions during storms, *J. Geophys. Res.*, *112*, A10220, doi:10.1029/2007JA012368.

Loto'aniu, T. M., I. R. Mann, L. G. Ozeke, A. A. Chan, Z. C. Dent, and D. K. Milling (2006), Radial diffusion of relativistic electrons into the radiation belt slot region during the 2003 Halloween geomagnetic storms, *J. Geophys. Res.*, *111*, A04218, doi:10.1029/2005JA011355.

Lyons, L. R. (1974), Electron diffusion driven by magnetospheric electrostatic waves, *J. Geophys. Res.*, *79*(4), 575–580.

Lyons, L. R., and R. M. Thorne (1973), Equilibrium structure of radiation belt electrons, *J. Geophys. Res.*, *78*(13), 2142–2149, doi:10.1029/JA078i013p02142.

Lyons, L. R., R. M. Thorne, and C. F. Kennel (1971), Electron pitch-angle diffusion driven by oblique whistler-mode turbulence, *J. Plasma Phys.*, *6*, 589–606, doi:10.1017/S0022377800006310.

Lyons, L. R., R. M. Thorne, and C. F. Kennel (1972), Pitch-angle diffusion of radiation belt electrons within the plasmasphere, *J. Geophys. Res.*, *77*(19), 3455–3474, doi:10.1029/JA077i019p03455.

Meredith, N. P., R. B. Horne, R. H. A. Iles, R. M. Thorne, D. Heynderickx, and R. R. Anderson (2002), Outer zone relativistic electron acceleration associated with substorm-enhanced whistler mode chorus, *J. Geophys. Res.*, *107*(A7), 1144, doi:10.1029/2001JA900146.

Meredith, N. P., R. M. Thorne, R. B. Horne, D. Summers, B. J. Fraser, and R. R. Anderson (2003), Statistical analysis of relativistic electron energies for cyclotron resonance with EMIC waves observed on CRRES, *J. Geophys. Res.*, *108*(A6), 1250, doi:10.1029/2002JA009700.

Meredith, N. P., R. B. Horne, S. A. Glauert, and R. R. Anderson (2007), Slot region electron loss timescales due to plasmaspheric hiss and lightning-generated whistlers, *J. Geophys. Res.*, *112*, A08214, doi:10.1029/2007JA012413.

Millan, R. M., and R. M. Thorne (2007), Review of radiation belt relativistic electron losses, *J. Atmos. Sol. Terr. Phys.*, *69*, 362–377.

Miyoshi, Y., A. Morioka, H. Misawa, T. Obara, T. Nagai, and Y. Kasahara (2003), Rebuilding process of the outer radiation belt during the 3 November 1993 magnetic storm: NOAA and Exos-D observations, *J. Geophys. Res.*, *108*(A1), 1004, doi:10.1029/2001JA007542.

Ni, B., R. M. Thorne, Y. Y. Shprits, and J. Bortnik (2008), Resonant scattering of plasma sheet electrons by whistler-mode chorus: Contribution to diffuse auroral precipitation, *Geophys. Res. Lett.*, *35*, L11106, doi:10.1029/2008GL034032.

O'Brien, T. P., K. R. Lorentzen, I. R. Mann, N. P. Meredith, J. B. Blake, J. F. Fennell, M. D. Looper, D. K. Milling, and R. R. Anderson (2003), Energization of relativistic electrons in the presence of ULF power and MeV microbursts: Evidence for dual ULF and VLF acceleration, *J. Geophys. Res.*, *108*(A8), 1329, doi:10.1029/2002JA009784.

Paulikas, G. A., J. B. Blake, and S. C. Freden (1967), Inner-zone electrons in 1964 and 1965, *J. Geophys. Res.*, *72*(7), 2011–2020, doi:10.1029/JZ072i007p02011.

Schulz, M., and L. J. Lanzerotti (1974), *Physics and Chemistry in Space*, vol. 7, *Particle Diffusion in the Radiation Belts*, 215 pp., Springer, New York.

Shea, M. A. (2006), Editorial comment, *Adv. Space Res.*, *38*(2), 115, doi:10.1016/j.asr.2006.09.002.

Sheeley, B., M. Moldwin, H. Rassoul, and R. Anderson (2001), An empirical plasmasphere and trough density model: CRRES observations, *J. Geophys. Res.*, *106*(A11), 25,631–25,641.

Shprits, Y. Y. (2009), Potential waves for pitch-angle scattering of near-equatorially mirroring energetic electrons due to the violation of the second adiabatic invariant, *Geophys. Res. Lett.*, *36*, L12106, doi:10.1029/2009GL038322.

Shprits, Y. Y., and B. Ni (2009), Dependence of the quasi-linear scattering rates on the wave normal distribution of chorus waves, *J. Geophys. Res.*, *114*, A11205, doi:10.1029/2009JA014223.

Shprits, Y. Y., and R. M. Thorne (2004), Time dependent radial diffusion modeling of relativistic electrons with realistic loss rates, *Geophys. Res. Lett.*, *31*, L08805, doi:10.1029/2004GL019591.

Shprits, Y. Y., R. M. Thorne, R. Friedel, G. D. Reeves, J. Fennell, D. N. Baker, and S. G. Kanekal (2006a), Outward radial diffusion driven by losses at magnetopause, *J. Geophys. Res.*, *111*, A11214, doi:10.1029/2006JA011657.

Shprits, Y. Y., W. Li, and R. M. Thorne (2006b), Controlling effect of the pitch angle scattering rates near the edge of the loss cone on electron lifetimes, *J. Geophys. Res.*, *111*, A12206, doi:10.1029/2006JA011758.

Shprits, Y. Y., R. M. Thorne, R. B. Horne, S. A. Glauert, M. Cartwright, C. T. Russell, D. N. Baker, and S. G. Kanekal (2006c), Acceleration mechanism responsible for the formation of the new radiation belt during the 2003 Halloween solar storm, *Geophys. Res. Lett.*, *33*, L05104, doi:10.1029/2005GL024256.

Shprits, Y. Y., R. M. Thorne, R. B. Horne, and D. Summers (2006d), Bounce-averaged diffusion coefficients for field-aligned chorus waves, *J. Geophys. Res.*, *111*, A10225, doi:10.1029/2006JA011725.

Shprits, Y. Y., N. P. Meredith, and R. M. Thorne (2007), Parameterization of radiation belt electron loss timescales due to interactions with chorus waves, *Geophys. Res. Lett.*, *34*, L11110, doi:10.1029/2006GL029050.

Shprits, Y. Y., S. R. Elkington, N. P. Meredith, and D. A. Subbotin (2008a), Review of modeling of losses and sources of relativistic electrons in the outer radiation belts I: Radial transport, *J. Atmos. Sol. Terr. Phys.*, *70*, 1679–1693, doi:10.1016/j.jastp.2008.06.008.

Shprits, Y. Y., D. A. Subbotin, N. P. Meredith, and S. R. Elkington (2008b), Review of modeling of losses and sources of relativistic electrons in the outer radiation belt II: Local acceleration and loss, *J. Atmos. Sol. Terr. Phys.*, *70*, 1694–1713, doi:10.1016/j.jastp.2008.06.014.

Shprits, Y. Y., D. Subbotin, and B. Ni (2009a), Evolution of electron fluxes in the outer radiation belt computed with the VERB code, *J. Geophys. Res.*, *114*, A11209, doi:10.1029/2008JA013784.

Shprits, Y. Y., L. Chen, and R. M. Thorne (2009b), Simulations of pitch angle scattering of relativistic electrons with MLT-dependent diffusion coefficients, *J. Geophys. Res.*, *114*, A03219, doi:10.1029/2008JA013695.

Starks, M. J., R. A. Quinn, G. P. Ginet, J. M. Albert, G. S. Sales, B. W. Reinisch, and P. Song (2008), Illumination of the plasmasphere by terrestrial very low frequency transmitters: Model validation, *J. Geophys. Res.*, *113*, A09320, doi:10.1029/2008JA013112.

Subbotin, D. A., and Y. Y. Shprits (2009), Three-dimensional modeling of the radiation belts using the Versatile Electron Radiation Belt (VERB) code, *Space Weather*, *7*, S10001, doi:10.1029/2008SW000452.

Subbotin, D., Y. Shprits, and B. Ni (2010), Three-dimensional VERB radiation belt simulations including mixed diffusion, *J. Geophys. Res.*, *115*, A03205, doi:10.1029/2009JA015070.

Summers, D., B. Ni, and N. P. Meredith (2007), Timescales for radiation belt electron acceleration and loss due to resonant wave-particle interactions: 2. Evaluation for VLF chorus, ELF hiss, and electromagnetic ion cyclotron waves, *J. Geophys. Res.*, *112*, A04207, doi:10.1029/2006JA011993.

Tsurutani, B. T., E. J. Smith, and R. M. Thorne (1975), Electromagnetic hiss and relativistic electron losses in the inner zone, *J. Geophys. Res.*, *80*(4), 600–607, doi:10.1029/JA080i004p00600.

Tsurutani, B. T., W. D. Gonzalez, G. S. Lakhina, and S. Alex (2003), The extreme magnetic storm of 1–2 September 1859, *J. Geophys. Res.*, *108*(A7), 1268, doi:10.1029/2002JA009504.

Tsurutani, B. T., et al. (2006), Corotating solar wind streams and recurrent geomagnetic activity: A review, *J. Geophys. Res.*, *111*, A07S01, doi:10.1029/2005JA011273.

Ukhorskiy, A. Y., B. J. Anderson, P. C. Brandt, and N. A. Tsyganenko (2006), Storm time evolution of the outer radiation belt: Transport and losses, *J. Geophys. Res.*, *111*, A11S03, doi:10.1029/2006JA011690.

Ukhorskiy, A. Y., Y. Y. Shprits, B. J. Anderson, K. Takahashi, and R. M. Thorne (2010), Rapid scattering of radiation belt electrons by storm-time EMIC waves, *Geophys. Res. Lett.*, *37*, L09101, doi:10.1029/2010GL042906.

Varotsou, A., D. Boscher, S. Bourdarie, R. B. Horne, S. A. Glauert, and N. P. Meredith (2005), Simulation of the outer radiation belt electrons near geosynchronous orbit including both radial diffusion and resonant interaction with whistler-mode chorus waves, *Geophys. Res. Lett.*, *32*, L19106, doi:10.1029/2005GL023282.

Varotsou, A., D. Boscher, S. Bourdarie, R. B. Horne, N. P. Meredith, S. A. Glauert, and R. H. Friedel (2008), Three-dimensional test simulations of the outer radiation belt electron dynamics including electron-chorus resonant interactions, *J. Geophys. Res.*, *113*, A12212, doi:10.1029/2007JA012862.

Vette, J. I. (1991), The AE-8 trapped electron model environment, *NSSDC/WDC-A-R&S 91-24*, NASA, Greenbelt, Md.

Walt, M. (1964), The effects of atmospheric collisions on geomagnetically trapped electrons, *J. Geophys. Res.*, *69*(19), 3947–3958, doi:10.1029/JZ069i019p03947.

Walt, M., and L. L. Newkirk (1968), *Earth's Particles and Fields*, 209 pp., Reinhold, New York.

D. Baker, LASP, University of Colorado at Boulder, Boulder, CO 80303, USA.

P. Cruce and Y. Shprits, Institute of Geophysics and Planetary Physics, University of California, Los Angeles, CA 90095, USA. (yshprits@atmos.ucla.edu)

R. Horne, British Antarctic Survey, Cambridge CB3 0ET, UK.

B. Ni and D. Subbotin, Department of Atmospheric and Oceanic Sciences, University of California, Los Angeles, CA 90095, USA.